

# Thermal dependence of the zero-bias conductance through a nanostructure

A. C. Seridonio,<sup>1</sup> M. Yoshida,<sup>2</sup> and L.N. Oliveira<sup>3</sup>

<sup>1</sup>*ICCP - International Center of Condensed Matter Physics  
Universidade de Brasília, 04513, Brasília, DF, Brazil*

<sup>2</sup>*Departamento de Física, Instituto de Geociências e Ciências Exatas,  
Universidade Estadual Paulista, 13500, Rio Claro, SP, Brazil*

<sup>3</sup>*Departamento de Física e Informática, Instituto de Física de São Carlos,  
Universidade de São Paulo, 369, São Carlos, SP, Brazil*

(Dated: May 26, 2019)

Motivated by the experimental observation of antiresonances in the conductance of a quantum wire coupled to a quantum dot, we show that, for gate potentials favoring the formation of dot magnetic moment, a linear mapping with known coefficients relates the temperature-dependent conductance through the wire or dot to the conductance through the dot for the symmetric Anderson model. We compare this expression with (i) essentially exact numerical-renormalization group results for various dot energies and Fano parameters; (ii) experimental data reported by Sato *et al.* [Phys. Rev. Lett. **95**, 066801 (2005).]

Three decades ago, the unraveling of the Kondo problem demonstrated that the physical properties of dilute magnetic alloys follow universal laws [1, 2], a finding subsequently born out in the laboratory [3, 4, 5, 6]. The revelation that many-body effects analogous to those found in such alloys should affect currents in nanodevices [7, 8] thus started a search for the universal function  $G_{univ}(T)$  that, in the wide range of gate voltages favoring the formation of a net magnetic moment in the dot, might guide the interpretation of future measurements. In this *Kondo range*, upon cooling, just as the host electrons screen the magnetic impurities in alloys, conduction electrons coupled to the dot should screen its moment. A properly chosen Kondo temperature  $T_K$ , dependent on couplings, interactions, band structure and other experimental details, should therefore make  $G_{univ}(T/T_K)$  match measured conductances.

Theory and experiment substantiated this program. Before the first *single-electron transistor* (SET), a quantum dot bridging two otherwise independent electron gases, was developed [9], a numerical renormalization-group (NRG) study of transport in dilute magnetic alloys had extracted  $G_{univ}(T/T_K)$  from the impurity spectral density for the symmetric Anderson model [10]. Accordingly, experimental curves were fitted with a parametrization of the numerical data for  $G_{univ}$  [11]:

$$\tilde{G}_{univ}(T/T_K) = G_{max} / (1 + (T/T'_K)^2)^s, \quad (1)$$

where  $G_{max} = \mathcal{G}_2 \equiv 2e^2/h$  (the quantum conductance),  $s = 0.22$ , and  $T'_K$  is such that  $\tilde{G}_{univ}(1) = G_{max}/2$ .

Near  $T_K$ ,  $G_{univ}(T)$  describes the conductance in the entire Kondo range [10]. At low temperatures, however, since  $G(T = 0) = \mathcal{G}_2 \sin^2 \delta$ , where  $\delta$  is the ground-state phase shift [12], only the phase shift  $\delta = \pi/2$  of the symmetric model [13] reaches the ballistic limit. The asymmetric models show disagreement with  $G_{univ}$  that grows with  $|\delta - \pi/2|$ . This mismatch and limitations that once kept experimental conductances well below  $\mathcal{G}_2$  led

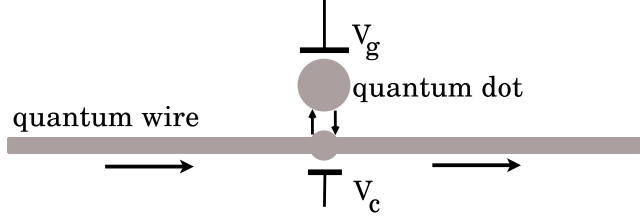


Figure 1: Quantum wire with side-coupled quantum dot. The gate potentials  $V_g$  and  $V_c$  control the energies of the dot level  $c_0$  and localized orbital  $f_0$  (shaded circle on the wire). The other two wire segments are coupled to  $c_0$  and  $f_0$ ; the ratio between the two couplings is proportional to a Fano parameter  $q$ , which partitions the indicated current between  $c_0$  and  $f_0$ .

to the practice of adjusting the parameters  $s$  and  $G_{max}$  in Eq. (1) to fit laboratory data [14, 15, 16, 17].

Recently, conductances were measured in the *side-coupled* setup [18, 19, 20] of Fig 1: a quantum dot coupled to a weakly biased quantum wire. While screening favors low-temperature transport in SETs, in the side-coupled geometry it drains charge from the wire and minimizes the low- $T$  conductance. Sato *et al.* [19, 20] thus adjusted  $G_{max}$  and  $s$  to fit the measured conductances with  $G_{off} - \tilde{G}_{univ}(T)$  ( $G_{off} = 0.9\mathcal{G}_2$  is their measured off-resonance conductance), an expedient justified by analysis: while the SET conductance depends on the spectral density of the dot, the side-coupled conductance depends on the complementary spectral density of the wire orbital coupled to the dot [21]. In the symmetric model, therefore, the side-coupled conductance is  $\mathcal{G}_2 - G_{univ}(T)$ .

In the side-coupled geometry, the currents through the wire and the dot tend to interfere [18]; even in SETs, Fano antiresonances have been reported [22]. Unfortunately, while fixed-temperature theories have provided qualitative understanding of the asymmetrical conductance vs. gate voltage plots [21, 23, 24, 25, 26, 27, 28, 29],

quantitative comparison has been plagued by the number of unknowns.

An alternative approach seems therefore desirable, and a physical notion provides one: an infinitesimal current cannot influence the formation of a Kondo cloud. With or without interference, we expect universality to prevail. To make this point, we show below that, in the Kondo range, the temperature dependence of the conductance and the universal function  $G_{univ}$  are always linearly related. Our analysis applies renormalization-group concepts to the single-level Anderson model for the device in Fig. 1, with a Fano parameter  $q$  describing the ratio between the amplitudes for electronic transfer through the dot and through the wire [30]. To explore this finding, we additionally discuss novel, essentially exact NRG results for the thermal dependence of the conductance for the Fano-Anderson model and compare those results with experimental data reported by Sato et al.[19].

*Model.* Conceptually, it is convenient to divide the wire in Fig. 1 into a central, localized state  $f_0$ , and a left ( $s = L$ ) and a right ( $s = R$ ) segments. Thus

$$H_w = \sum_{ks} \epsilon_k c_{sk}^\dagger c_{sk} + 2t (f_0^\dagger f_1 + \text{H. c.}), \quad (2)$$

where we have omitted spin indices and adopted the shorthand  $f_1 \equiv \sum_{ks} c_{ks}/2$ . The conduction states  $c_{sk}$  ( $s = L, R$ ) obey the dispersion relation  $\epsilon_k = v_F(k - k_F)$ , where  $v_F$  ( $k_F$ ) is the Fermi velocity (momentum) and the energies  $\epsilon_k$ , measured from the Fermi level, extend from  $-D$  to  $D$ . As long as  $t \approx D$ , only irrelevant operators separate  $H_w$  from the undivided-wire Hamiltonian.

The quantum-dot level  $c_0$  is coupled to both the central wire state  $f_0$  and the lateral states, with relative amplitudes defined by a (complex) Fano-parameter  $q$  [30]:

$$H_{wd} = V c_0^\dagger (f_0 + 2\pi q(t/D) f_1) + \text{H. c..} \quad (3)$$

In the dot Hamiltonian,  $H_d = \epsilon_0 n_0 + U n_{0\uparrow} n_{0\downarrow}$ , the gate voltage  $V_g$  controls the dot-level energy  $\epsilon_0$ , and competes with the Coulomb repulsion  $U$  ( $U \geq -\epsilon_0 \geq 0$ ) to fix the occupation  $n_0$ . The model Hamiltonian combines  $H_d$  with Eqs. (2) and (3) [31]:

$$H_A = \sum_{ks} \epsilon_k c_{sk}^\dagger c_{sk} + (2t \mathcal{N}_q d_q^\dagger f_1 + V f_0^\dagger c_0 + \text{H. c.}) + H_d, \quad (4)$$

where  $\mathcal{N}_q \equiv \sqrt{1 + (\pi|q|V/D)^2}$  normalizes the Fermi operator  $d_q \equiv [f_0 + (\pi q V/D) c_0]/\mathcal{N}_q$ .

Kubo's formula [32] yields the zero-bias conductance:

$$G_q(T) = \mathcal{G}_2 \int_{-D}^D D\rho_q(\epsilon, T) \left[ -\frac{\partial f(\epsilon)}{\partial \epsilon} \right] d\epsilon, \quad (5)$$

where  $f(\epsilon)$  is the Fermi function,

$$\rho_q(\epsilon, T) = \sum_{m,n} \frac{e^{-\beta E_m}}{f(-\epsilon) \mathcal{Z}} |\langle n | d_q | m \rangle|^2 \delta(\epsilon - E_m + E_n) \quad (6)$$

is the spectral density for  $d_q$ ,  $\mathcal{Z}$  is the partition function, and  $|m\rangle$  ( $E_m$ ) is an eigenstates (eigenvalue) of  $H_A$ . Substitution of Eq. (6) for  $\rho_q$  in Eq. (5) yields

$$G_q(T) = \frac{\mathcal{G}_2 D}{k_B T \mathcal{Z}} \sum_{m,n} \frac{|\langle n | d_q | m \rangle|^2}{\exp(\beta E_m) + \exp(\beta E_n)}. \quad (7)$$

*Analysis.* We are interested in the Kondo range. Here, the energetic cost  $\Delta_- = -\epsilon_0$  ( $\Delta_+ = U + \epsilon_0$ ) of removing (adding) one electron from (to) the dot dwarves the level width:  $k_B T_\pm \equiv \min(\Delta_+, \Delta_-) \gg \Gamma \equiv 2\pi V^2/D$ . In this range, for temperatures  $T$  such that  $T_\pm \gg T \gg T_K$ , the Hamiltonian (4) lies near the *local-moment* line of fixed points. The wire phase shift  $\delta_{LM}$ , which reflects the asymmetry between  $\Delta_+$  and  $\Delta_-$ , labels each fixed point [13]. In the symmetric model ( $\epsilon_0 = -U/2$ ) the phase shift vanishes because  $\Delta_+ = \Delta_-$  [2, 31]; for other level energies, the single-particle eigenvalues of  $H_A$  yield  $\delta_{LM}$  [13].

Given that the fixed points are non-interacting Hamiltonians, we apply standard Green's functions techniques to the right-hand side of Eq. (6) and, with the definition  $\tan \delta_q \equiv q$  (to make our expressions compact, we initially consider real  $q$ 's), we find  $\rho_q(LM) = \cos^2(\delta_{LM} - \delta_q)$ . From Eq. (5) we then have that

$$G_q(T) = \mathcal{G}_2 \cos^2(\delta_{LM} - \delta_q) \quad (T \ll T_\pm). \quad (8)$$

In practice, the model Hamiltonian never reaches the local-moment fixed point, for upon cooling the coupling between the dot moment and the conduction spins drives it away toward the line of *frozen-level* fixed points [13]. Each of these is also labeled by a phase shift  $\delta = \delta_{LM} + \pi/2$ , an equality imposed by the Friedel sum rule [12]. Again, standard techniques determine the spectral density  $\rho_q$  [12], and we recover Eq. (8) with  $\delta$  substituted for  $\delta_{LM}$  [23], i. e.,

$$G_q(T) = \mathcal{G}_2 \begin{cases} \sin^2(\delta - \delta_q) & (T_K \ll T \ll T_\pm) \\ \cos^2(\delta - \delta_q) & (T \ll T_K) \end{cases} \quad (9)$$

To discuss the crossover from the local-moment to the frozen-level fixed points we refer to Costi's et al.'s NRG study of the impurity spectral density, i. e., of  $\rho_{q \rightarrow \infty}(\epsilon, T)$  [10]. Chiefly important is their result for the  $q \rightarrow \infty$  limit of the integral on the right-hand side of Eq. (5) for the symmetric model ( $\epsilon_0 = -U/2$ ), which we denote  $g_\infty^s(T)$ .

We want to show that  $g_\infty^s(T/T_K)$  determines  $G_q(T)$  over the entire Kondo range. To that end we note that, since the local-moment phase shift (the Fano parameter) is associated with the strictly marginal (irrelevant) operator  $f_0^\dagger f_0$  ( $c_0^\dagger f_1$ ) [1, 13], the temperature-dependent conductance for the Hamiltonian (4) is universal. Most generally, it has the form

$$G_q(T/T_K) = \mathcal{G}_2 (A(\delta, \delta_q) + B(\delta, \delta_q) \phi(T/T_K)), \quad (10)$$

where the two independent parameters  $A$  and  $B$  leave us free to choose the two extremes,  $\phi(0) = 1$  and  $\phi(\infty) = 0$ , of the as yet unknown universal function  $\phi$ . With  $T = 0$ , Eq. (9) then implies  $A + B = \cos^2(\delta - \delta_q)$  and, with  $T \gg T_K$ ,  $A = \sin^2(\delta - \delta_q)$ , so that Eq. (10) reads

$$G_q\left(\frac{T}{T_K}\right) = \frac{\mathcal{G}_2}{2} \left[ 1 - \left( 1 - 2\phi\left(\frac{T}{T_K}\right) \right) \cos 2(\delta - \delta_q) \right]. \quad (11)$$

In particular, if  $H_A$  is the symmetric Hamiltonian and  $q \rightarrow \infty$ , then  $\delta = \delta_q = \pi/2$  and Eq. (11) reduces to  $G(T/T_K) = \mathcal{G}_2\phi(T/T_K)$ . Comparison with our definition  $G_{q \rightarrow \infty}(T/T_K) \equiv \mathcal{G}_2 g_\infty^s(T/T_K)$  shows that the universal function  $\phi$  is none other than  $g_\infty^s$ . With the notation  $F_\delta^q = \cos 2(\delta - \delta_q)$ , Eq. (11) becomes

$$G_q(T/T_K) = (\mathcal{G}_2/2) [1 + F_\delta^q (2g_\infty^s(T/T_K) - 1)]. \quad (12)$$

For complex Fano parameters, the same reasoning with  $q \equiv |q| \exp(i\varphi)$  and  $\tan \delta_q \equiv |q|$  recovers Eq. (12) with

$$F_\delta^q = \cos 2\delta \cos 2\delta_q + \cos \varphi \sin 2\delta \sin 2\delta_q. \quad (13)$$

In the Kondo range, for all  $q$  and  $T \ll T_\pm$ , the linear Eq. (12) therefore ties the conductance to  $g_\infty^s(T/T_K)$ . Hereafter we discuss a few implications of this relation.

*Real Fano parameters.* We diagonalized the model Hamiltonian and computed the right-hand side of Eq. (7) from the resulting eigenvalues and eigenvectors. In a typical run of our NRG procedure [33] (maximum of 5100 lowest-energy states kept in each iteration,  $\Lambda = 6$ , conductances averaged over two  $z$ 's [34]: 0.5 and 1), a desktop machine takes less than 1 minute to generate a complete  $G_q(T)$  curve, with less than  $0.01e^2/h$  deviation at any temperature.

We report conductances for six dot-level energies:  $-\varepsilon_0/\Gamma = 1.2, 2, 5, 9, 15$ , and  $23$ , with fixed width  $\Gamma = 0.01D$  and Coulomb repulsion  $U = 0.3D$ . The symmetric dot energy  $\varepsilon_0 = -15\Gamma$  bisects the Kondo range  $-5\Gamma \gtrsim \varepsilon_0 \gtrsim -25\Gamma$ . For each  $\varepsilon_0$ , we extracted the phase shift  $\delta$  from the numerically computed single-particle eigenvalues of the frozen-level Hamiltonian [13]. As expected, as  $\varepsilon_0$  sweeps the Kondo range, the sluggish displacement of the Kondo resonance across the Fermi level binds the phase shift to the vicinity of  $\pi/2$ : it runs from  $\delta = 0.464\pi$ , at  $\varepsilon_0 = -5\Gamma$ , to  $\delta = 0.536\pi$ , at  $\varepsilon_0 = -25\Gamma$ .

Figure 2 shows the temperature dependence of  $G_{q \rightarrow \infty}$ . The solid line is the universal function  $g_\infty^s \equiv G_\infty/\mathcal{G}_2$ , i. e., the conductance for the symmetric model, from which Eq. (12) produces all the dotted lines in the main plot and insets. The open diamonds, tilted crosses and filled rectangles show computed conductances for  $\varepsilon_0 = -1.2\Gamma$  and  $-2\Gamma$ , outside the Kondo range, and the borderline energy  $\varepsilon_0 = -5\Gamma$ , respectively. Since  $G_\infty$  remains invariant under the (particle-hole) transformation  $\Delta_+ \rightarrow \Delta_-$ , these curves also represent  $\varepsilon_0 = -28.8\Gamma, -28\Gamma$ , and  $-25\Gamma$ , respectively.

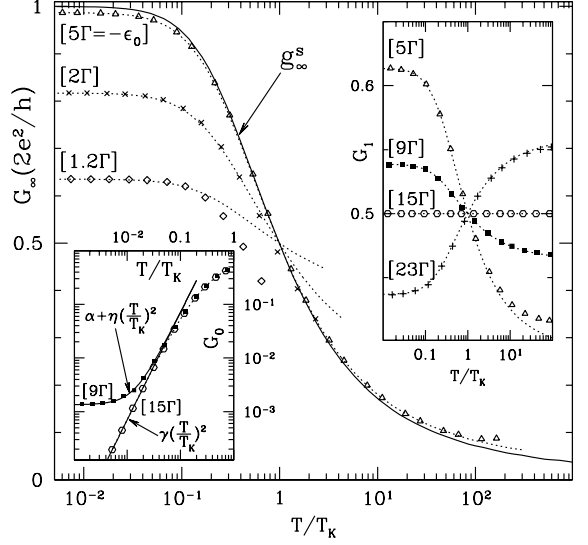


Figure 2: Conductance vs. temperature for  $\Gamma = 0.01D$ ,  $U = 0.3D$  and the indicated  $\varepsilon_0$ 's. In the main plot, Fano parameter  $q \rightarrow \infty$  ( $2\delta_q = \pi$ ), the solid line runs through the computed conductances for the symmetric model. The triangles, crosses and diamonds display other computations. In all plots, the dotted lines are Eq. (12) with  $F_\delta^q = \cos(2\delta - 2\delta_q)$  and phase shifts  $\delta$  obtained from the single-particle eigenvalues of the frozen-level fixed point for the pertinent  $\varepsilon_0$ . The top-right inset show conductances for  $q = 1$  ( $4\delta_q = \pi$ ), the bottom-left one, for  $q = \delta_q = 0$ . In the latter, the straight and the parabolic solid lines represent Eq. (14)

For  $\varepsilon_0 = -1.2\Gamma$ , with a phase shift  $\delta = 0.206\pi$  significantly smaller than  $\pi/2$ , only at the lowest temperatures is there agreement with Eq. (11). Closer to the Kondo range, however, the congruence rapidly expands to higher temperatures: even for excitation energies  $\Delta_-$  only twice as large as the width  $\Gamma$ , the crosses show coincidence below the Kondo temperature, and for  $\Delta_- = 5\Gamma$ , the mismatch is restricted to temperatures well above  $T_K$ . In the Kondo range, with  $q \rightarrow \infty$ , the phase  $\delta_q = \pi/2$  places  $F_\delta^q = \cos 2(\delta - \delta_q)$  close to unity and, upon heating, makes the conductance decay from nearly the ballistic limit to nearly zero along curves that need not be displayed, for the scale of the plot makes them indistinguishable from  $g_\infty^s(T)$ . First seen in Ref. 10, often exploited in the interpretation of experimental data [14, 15, 16, 17], and responsible for the appearance of *Kondo plateaus* in  $G$  vs.  $\varepsilon_0$  plots [35], this insensitivity of  $G_\infty(T)$  to the gate voltage, more than a mere consequence of universality, relies on the the composition of two effects: (1) the weak dependence of  $\delta$  on  $\varepsilon_0$  in the Kondo range; (2) the proximity of  $F_\delta^q$  to a maximum.

In the top-right inset, the more expanded vertical scale displays better the agreement with Eq. (12) within the

Kondo range and of the small high-temperature deviations at a borderline dot energy ( $\varepsilon_0 = -5\Gamma$ ). Here, with  $q = 1$ , electrons can run through the wire OR through the dot. At low temperatures, the Kondo cloud obstructs the wire, and current flows through the dot; at high temperatures, the Coulomb blockade arises in the dot, and current flows through the wire. The alternative paths flatten the thermal dependence of the conductance. In particular, for  $\varepsilon_0 = -U/2$  (circles), particle-hole symmetry rules out interference and makes the conductance temperature independent. For  $|\varepsilon_0| < U/2$  (squares and triangles), the two currents interfere constructively below the Kondo temperature and destructively above it, so that the conductance decays with temperature. For  $|\varepsilon_0| > U/2$  (crosses), this pattern is reversed. This shows that, even in the Kondo range, the thermal dependence depends markedly on the gate voltage; if shown, fixed-temperature plots of  $G_1$  vs.  $\varepsilon_0$  would display the askew profile characteristic of Kondo antiresonances [30].

In the other inset, the logarithmic representation inspects the low-temperature conductance through the wire, the only channel available with  $q = 0$ . At low temperatures the Kondo cloud blocks conductance, which hence rises upon heating. As in the main plot, the dependence on the gate voltage is weak, because  $F_\delta^q$  is near a minimum,  $F_\delta^q \approx -1$ . From the low-temperature behavior of the resistivity for the Anderson model [36] and Eq. (12) we extract the exact asymptotic expression

$$G_q(T \rightarrow 0) = \frac{\mathcal{G}_2}{2} (1 - F_\delta^q + 2\gamma F_\delta^q (T/T_K)^2). \quad (14)$$

The coefficient  $\gamma$  depends on the definition of  $T_K$ . With a Kondo temperature  $T_K^{Noz}$  such that the zero-temperature susceptibility of the Kondo model is  $\chi(T = 0) = (g\mu_B)^2/(4T_K^{Noz})$ , Nozières found  $\gamma_{Noz} = \pi^4/16$ . Our definition,  $G_q(T_K) = \mathcal{G}_2/2$  yields  $\chi(T = 0) = 0.268(g\mu_B)^2/T_K$ , so that  $T_K = (4 \times 0.268)T_K^{Noz}$  and  $\gamma = (4 \times 0.268)^2\gamma_{Noz} = 7.00$ . With  $q = 0$ , Eq. (14) becomes  $G_0 = \mathcal{G}_2[\alpha + \eta(T/T_K)^2]$ , where  $\alpha = \cos^2\delta$  and  $\eta = \gamma \cos 2\delta$ . The agreement between the straight (parabolic) solid line representing this equality and the circles (squares) confirms that, at any given temperature, our computed conductances are reliable within  $0.01e^2/h$ .

*Complex  $q$ .* The phase  $\varphi$  of the Fano parameter partially destroys the coherence between the currents through the wire and through the dot and dampens their interference. As a result, neither the ballistic nor the insulating limits can be achieved. The conductance is more strictly bounded:  $|G_q(T) - \mathcal{G}_2/2| < \mathcal{G}_2 F_\delta^q$ , where  $\bar{F}_\delta^q \equiv \sqrt{1 - \sin^2(2\delta_q) \sin^2(\varphi)}$  [37].

*Experiment.* The linear form makes Eq. (12) convenient for quantitative comparisons. Given a set of experimental points  $S_{\text{exptal}} \equiv \{G_i, T_i\}$  ( $i = 1, \dots, N$ ), one can choose a trial Kondo temperature  $T_K^{\text{trial}}$  and generate a set of dimensionless temperatures  $\tau_i = T_i/T_K^{\text{trial}}$ ,

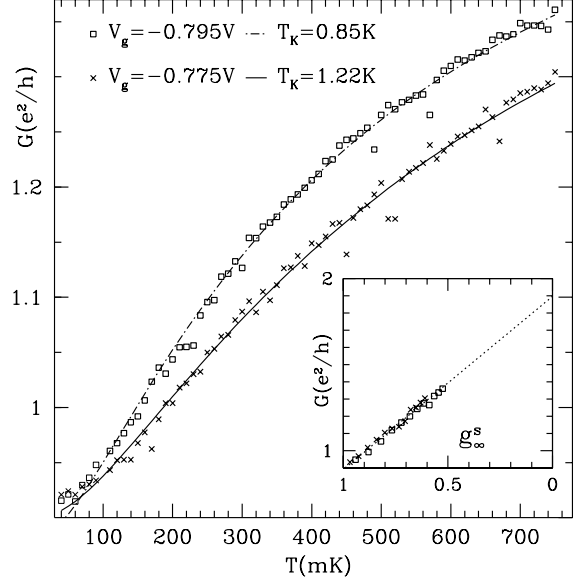


Figure 3: Theory compared with experiment [19]. The crosses and squares are the conductances  $G$  measured at the indicated gate potentials  $V_g$ ; temperature measurements below 100mK involve large uncertainties [19]. The inset, whose horizontal axis runs from 1 to 0 as a reminder that  $g_\infty^s(T = 0) = 1$ , shows that each indicated Kondo temperature straightens the corresponding plot of  $G$  vs.  $g_\infty^s$ . The linear-regression representation of each such line, Eq. (15), is shown as a function of temperature in the main plot, compared with the experimental points.

( $i = 1, \dots, N$ ). This done, one inverts the function  $g_\infty^s$ , in Fig. 2, to determine the universal conductance  $g_\infty^s$  associated with each  $\tau_i$  ( $i = 1, \dots, N$ ). If the resulting plot of  $G_i$  vs.  $g_\infty^s$  is a straight line,  $T_K^{\text{trial}}$  is the Kondo temperature. If not, the procedure is iterated. Visual inspection determines the Kondo temperature within 10% error; numerical evaluation of the curvature makes this deviation as small as the dispersion of the experimental data. The inset in Fig. 3 applies this procedure to conductance data in Fig. 3b of Ref. 19, measured with the gate potentials  $V_g = -795\text{mV}$  (squares) and  $-775\text{mV}$  (crosses), and yields the Kondo temperatures  $T_K = 850\text{mK}$  and  $1230\text{mK}$ , respectively.

The coefficients of the straight line resulting from the  $G_i$  vs.  $g_\infty^s$  plot determined, reversal of the process provides a continuous function of temperature that can be compared with  $S_{\text{exptal}}$ . The agreement in the main plot confirms that the conductances were measured in the Kondo range. The dash-dotted and the solid curve are described by the expression

$$2G(T/T_K) = \mathcal{C}\mathcal{G}_2[1 + 0.36(1 - 2g_\infty^s(T/T_K))] \quad (15)$$

with the coefficients  $\mathcal{C} = 1.38$  and  $\mathcal{C} = 1.41$ , for  $V_g = -0.795\text{V}$  and  $V_g = -0.775\text{V}$ , respectively. At high tem-

peratures ( $g_\infty^s = 0$ ), in both cases, Eq. (15) yields  $G(T \gg T_K) \approx 1.9e^2/h$ , consistent with the experimental finding that the off-resonance conductance is approximately  $1.8e^2/h$  [19]. The difference in prefactors accounted for [37], comparison with Eq. (12) gives  $F_\delta^q = 0.36$ . The weak gate-voltage dependence shows that  $F_\delta^q$  is an extremum,  $F_\delta^q = \bar{F}_\delta^q$ , i. e.,  $\sqrt{1 - \sin^2(2\delta_q)} \sin^2 \varphi = 0.36$ , an equality that only  $|q| \approx 1$  AND  $\varphi \approx \pi/2$  can satisfy.

Finally, we observe that the residual conductance  $G(T \ll T_K) \approx 0.9e^2/h$  by no means indicates failure to screen the dot moment. The horizontal insert axis monitors the Kondo effect:  $g_\infty^s = 1$  is full screening. The convergence of the squares and crosses to that limit evidences the formation of a singlet at low temperatures.

We are grateful to Drs. Alvaro Ferraz, Vivaldo L. Campo, and V. V. Ponomarenko for stimulating conversations and to Prof. Shingo Katsumoto for sending us the data depicted in Fig. 3. This work was supported by the CNPq, FAPESP, and IBEM (Brazil).

---

[1] K. G. Wilson, Rev. Mod. Phys. **47**, 773 (1975).  
 [2] H. R. Krishna-murthy, J. W. Wilkins, and K. G. Wilson, Phys. Rev. B **21**, 1003 (1980).  
 [3] N. Andrei, K. Furuya, and J. H. Lowenstein, Rev. Mod. Phys. **55**, 331 (1983).  
 [4] A. M. Tsvelick and P. B. Wiegmann, Advances in Physics **32**, 453 (1983).  
 [5] C. L. Lin, A. Wallash, J. E. Crow, T. Mihalisin, and P. Schlottmann, Phys. Rev. Lett. **58**, 1232 (1987).  
 [6] A. C. Hewson, *The Kondo Problem to Heavy Fermions* (Cambridge University Press, Cambridge, 1993).  
 [7] L. I. Glazman and M. E. Raikh, JETP Lett. **47**, 452 (1987).  
 [8] T. K. Ng and P. A. Lee, Phys. Rev. Lett. **61**, 1768 (1988).  
 [9] D. Goldhaber-Gordon, H. Shtrikman, D. Mahalu, D. Abusch-Magder, U. Meirav, and M. A. Kastner, Nature **391**, 156 (1998).  
 [10] T. Costi, A. Hewson, and V. Zlatic, Journal of Physics B-Condensed Matter **6**, 2519 (1994).  
 [11] D. Goldhaber-Gordon, J. Gores, M. A. Kastner, H. Shtrikman, D. Mahalu, and U. Meirav, Phys. Rev. Lett. **81**, 5225 (1998).  
 [12] D. C. Langreth, Phys. Rev. **150**, 516 (1966).  
 [13] H. R. Krishna-murthy, J. W. Wilkins, and K. G. Wilson, Phys. Rev. B **21**, 1044 (1980).  
 [14] D. Goldhaber-Gordon, J. Gores, M. A. Kastner, H. Shtrikman, D. Mahalu, and U. Meirav, Phys. Rev. Lett. **81**, 5225 (1998).  
 [15] W. G. van der Wiel, S. D. Francheschi, T. Fujisawa, J. M. Elzerman, S. Tarucha, and L. P. Kouwenhoven, Science **289**, 2105 (2000).  
 [16] S. M. Cronenwett, H. J. Lynch, D. Goldhaber-Gordon, L. P. Kouwenhoven, C. M. Marcus, K. Hirose, N. S. Wingreen, and V. Umansky, Phys. Rev. Lett. **88**, 226805 (2002).  
 [17] W. Liang, M. P. Shores, M. Bockrath, and J. R. Long, Nature **417**, 725 (2002).  
 [18] K. Kobayashi, H. Aikawa, A. Sano, S. Katsumoto, and Y. Iye, Phys. Rev. B **70**, 035319 (2004).  
 [19] M. Sato, H. Aikawa, K. Kobayashi, S. Katsumoto, and Y. Iye, Phys. Rev. Lett. **95**, 066801 (2005).  
 [20] S. Katsumoto, M. Sato, H. Aikawa, and Y. Iye, Physica E: Low-dimensional Systems and Nanostructures **34**, 36 (2006).  
 [21] I. Maruyama, N. Shibata, and K. Ueda, Journal of the Physical Society of Japan **73**, 3239 (2004).  
 [22] J. Göres, D. Goldhaber-Gordon, S. Heermeyer, M. A. Kastner, H. Shtrikman, D. Mahalu, and U. Meirav, Phys. Rev. B **62**, 2188 (2000).  
 [23] W. Hofstetter, J. König, and H. Schoeller, Phys. Rev. Lett. **87**, 156803 (2001).  
 [24] B. R. Bulka and P. Stefański, Phys. Rev. Lett. **86**, 5128 (2001).  
 [25] K. Kang, S. Y. Cho, J.-J. Kim, and S.-C. Shin, Phys. Rev. B **63**, 113304 (2001).  
 [26] M. E. Torio, K. Hallberg, A. H. Ceccatto, and C. R. Proetto, Phys. Rev. B **65**, 085302 (2002).  
 [27] O. Entin-Wohlman, A. Aharony, and Y. Meir, Phys. Rev. B **71**, 035333 (2005).  
 [28] B. H. Wu, J. C. Cao, and K.-H. Ahn, Phys. Rev. B **72**, 165313 (2005).  
 [29] I. Maruyama, N. Shibata, and K. Ueda, Physica B: Condensed Matter **378-380**, 938 (2006).  
 [30] U. Fano, Phys. Rev. **124**, 1866 (1961).  
 [31] The potential  $V_c$  in Fig. 1 may add a nonresonant scattering  $Kf_0^\dagger f_0$  to Eq. (4), which will displace the phase shifts, but in no other way affect our analysis.  
 [32] G. D. Mahan, *Many Particle Physics* (Plenum Press, New York, 1990).  
 [33] M. Yoshida, M. A. Whitaker, and L. N. Oliveira, Phys. Rev. B **41**, 9403 (1990).  
 [34] S. C. Costa, C. A. Paula, V. L. Libero, and L. N. Oliveira, Phys. Rev. B **55**, 30 (1997).  
 [35] N. S. Wingreen and Y. Meir, Phys. Rev. B **49**, 11040 (1994).  
 [36] P. Nozières, J. Low Temp. Phys. **17**, 31 (1975).  
 [37] Should an external potential force the conductance to reach the unitary limit, the right-hand side of Eq. (12) must be divided by  $(1 + \bar{F}_\delta^q)/2$ , and instead of  $\mathcal{G}_2/2$ , its prefactor will be  $\mathcal{G}_2/(1 + \bar{F}_\delta^q)$ .